

PCI-MF: Partial Canonical Identity and Matrix Factorization Framework for Channel Estimation in mmWave Massive MIMO Systems

NEHA JAIN ^{1,2,3}, VIVEK ASHOK BOHARA ^{1,2}, AND ANUBHA GUPTA ^{1,3}

¹ Department of Electronics and Communication Engineering, Indraprastha Institute of Information Technology, New Delhi, (IIIT-D) 110020, India

² Wirocomm Research Group, Delhi 110020, India

³ Signal Processing and Biomedical Imaging Lab (SBILab), Delhi 110020, India

CORRESPONDING AUTHOR: NEHA JAIN (e-mail: nehaj@iiitd.ac.in)

ABSTRACT Beamforming using massive number of antennas in millimeter wave (mmWave) communication is a promising solution for providing gigabits-per-second data rates in cellular networks. However, perfect channel state information (CSI) estimation is a key requirement, which is not practically feasible in massive multiple-input-multiple-output (MIMO) systems. Hence, compressive sensing (CS) and matrix completion methods have been proposed in the literature to reduce the channel estimation overhead. In this paper, a novel method utilizing partial canonical identity (PCI) based CS and matrix factorization (MF) framework, henceforth termed as PCI-MF, has been proposed to recover complete mmWave CSI by estimating only a few channel coefficients. Specifically, a few estimated noisy channel coefficients are represented as a combination of PCI and discrete Fourier transform (DFT) matrix in a CS framework to recover the sparsest solution of the channel matrix. This framework exploits the fact that both PCI and DFT matrices are highly incoherent. The sparse matrix determined above has been used to recover the rank of the channel matrix. The knowledge of the rank, along with the sparse coefficients recovered above, have been used jointly in a matrix factorization framework to recover the actual channel matrix. PCI-MF has been compared with the conventional and the state-of-the-art methods for two different datasets by varying parameters such as the number of transmitting and receiving antennas, antenna configuration, signal-to-noise ratio and measurement ratio. In order to validate the proposed method for realistic applications, one dataset is generated in a real-world setting in the New York City.

INDEX TERMS Millimeter wave, beamforming, multiple-input-multiple-output systems, partial canonical identity matrix, discrete Fourier transform, matrix factorization.

I. INTRODUCTION

To facilitate the vision of fifth-generation (5G) cellular standard, numerous advanced technologies such as shrinking the cell's size and advanced multiple-input-multiple-output (MIMO) have been proposed in the literature [1], [2]. However, the existing microwave band (<6 GHz) is mostly occupied and may not be able to meet future demands even after employing these technologies [3], [4]. Therefore, there is a need to move to extremely high frequency (EHF) band (30–300 GHz), also known as millimetre wave (mmWave)

band, which has the capability of providing data rates in giga-bits-per-second (Gbps) [5], [6]. The transmission at such high frequency comes at the expense of significant path attenuation [7]. Therefore, to overcome the propagation losses at mmWave frequencies, directional beamforming between transmitter and receiver is employed by using multiple antennas at both transmitter as well as receiver [8], [9]. Fortunately, due to shorter wavelength of mmWave communication system, more antennas can be placed together in a small area because the separation required between consecutive

antennas is around half of the signal's wavelength at both the transmitter as well as the receiver [10]. However, to provide sufficient beamforming gain, a well-aligned narrow beam between transmitter and receiver is required, which requires perfect channel state information (CSI). Since mmWave massive MIMO system utilizes multiple antennas at both transmitter and receiver, estimation of channel coefficients between every pair increases the overhead considerably.

To reduce the overhead, the problem of channel estimation in mmWave massive MIMO is formulated as either beam-alignment problem or compressive sensing (CS) problem. In beam alignment, the transmitter and receiver search for the best beam pair, which increases the feedback overhead [11]–[13]. However, the CS problem exploits the sparse behaviour of mmWave channel [14]–[16] and does not require feedback. Consequently, a few compressive measurements are obtained to recover the entire CSI by using sparse recovery methods, such as orthogonal matching pursuit (OMP) [17]. Apart from CS based techniques that exploit the sparse behaviour of mmWave channel, [18], [19] have exploited the low-rank property of mmWave channel to recover the CSI. In [18], [19] low-rank tensor factorization methods have been employed, which improve the accuracy and reduce the complexity as compared to the sparsity-based CS techniques. Recently, researchers have exploited both low-rank as well as sparse behaviour of mmWave channel to considerably improve the accuracy of the estimated CSI [20], [21]. In [20], a two-stage method has been developed for mmWave channel estimation, where the low-rank property in a matrix completion framework [22] and the sparse property in a sparse recovery framework have been used in two consecutive stages. Unlike above, in [21] both low-rank as well as the sparse property of mmWave channel matrix have been exploited jointly to obtain the entire CSI from a few channel coefficients. It uses an alternating direction method of multipliers (ADMM) for jointly exploiting the low-rank and sparse properties in a matrix completion framework. Simulations show considerable improvement in channel estimation in [21] as compared to [20].

The performance of existing methods is still restricted because these methods are not leveraging the known properties of mmWave massive MIMO channel matrix judiciously. In this paper, a joint framework utilizing partial canonical identity (PCI) based CS and matrix factorization (MF) named as “*PCI-MF*” has been proposed to recover complete CSI from a few noisy mmWave channel coefficients. The mmWave channel matrix is modeled as a two dimensional discrete Fourier transform (DFT) form of a sparse matrix due to the directional beamforming [23]. Since PCI and DFT matrices are mutually incoherent, the Fourier representation of the channel matrix is utilized in PCI based CS framework to estimate the sparse matrix associated with the channel matrix in the DFT domain. The rank of the channel matrix (or the number of dominant paths) is estimated by calculating the number of non-zero coefficients in the above estimated sparse matrix. This estimated rank and sparse coefficients have been used

jointly in a MF framework to recover the channel matrix. The main contributions of the proposed method, PCI-MF have been summarized below:

- Unlike the existing algorithm of [24], PCI-MF is not constrained that the *number of minimum transmissions during training phase* should be greater than or equal to the total number of transmitter antennas (N_T). Hence, it can estimate the full CSI from a few channel coefficients.
- PCI-MF has been shown to estimate the massive MIMO mmWave channel more accurately as compared to recent state-of-the-art algorithms such as [20], [21] and hence, provides a better achievable spectrum efficiency (ASE) for a mmWave MIMO communication system. For instance, it has been shown that at 25 dB SNR and 32×32 MIMO configuration, PCI-MF is able to achieve ASE of 16.09 bits/sec/Hz with only 30% of CSI, which is comparable to ASE achieved when full CSI is available.
- The improvement in the performance of PCI-MF has also been verified against numerous parameters such as antenna configuration (uniform linear array, uniform planar array), MIMO configurations (32×32 , 64×64), operating frequencies (28 GHz, 92 GHz) and fading channel models (Rayleigh fading and Nakagami fading).
- Results have also been verified on realistic data given in [25], [26]. PCI-MF is obtaining 5.45 dB and 16.93 dB improvement with 10% and 90% availability of channel information as compared to the existing methods.

Notations: \mathbf{X}' , \mathbf{X}^* and \mathbf{X}^H denote the transpose, conjugate, and the Hermitian (conjugate transpose) of matrix \mathbf{X} , respectively. The element corresponding to the i^{th} row and j^{th} column of a matrix \mathbf{X} is represented by $X(i, j)$. The i^{th} element of a vector \mathbf{x} is represented as $x(i)$. The vectorization of matrix \mathbf{X} is denoted as $\mathbf{X}(\cdot)$. \mathcal{D}_a is a normalized DFT matrix of size $a \times a$. $\mathbf{X} \otimes \mathbf{Y}$ and $\mathbf{X} \odot \mathbf{Y}$ represent the Kronecker and Hadamard products between matrices \mathbf{X} and \mathbf{Y} , respectively. The l^p norm of a matrix or a vector is represented as $\|\cdot\|_p$. Binary, complex and real matrices of size $a \times b$ are represented by $\mathbb{B}^{a \times b}$, $\mathbb{C}^{a \times b}$ and $\mathbb{R}^{a \times b}$, respectively. A random variable Z with Gaussian distribution with mean μ_g and variance σ_g^2 is represented as $Z \sim \mathcal{N}(\mu_g, \sigma_g^2)$. Similarly, the complex Gaussian random variable will be represented as $Z \sim \mathcal{CN}(\mu_g, \sigma_g^2)$. An exponentially distributed random variable Z with mean λ_e^{-1} is denoted as $Z \sim \mathcal{E}(\lambda_e)$. The Rayleigh distribution with variance σ_r^2 is represented as $Z \sim \mathcal{R}(\sigma_r^2)$. Further, a random variable with the Nakagami distribution is denoted as $Z \sim \mathcal{NG}(m, \Omega)$, where m is the shape parameter and Ω is the controlling parameter. Moreover, Poisson distribution with mean μ_{po} and Laplace distribution with standard deviation σ_{lp} are represented as $Z \sim \mathcal{P}(\mu_{po})$ and $Z \sim \mathcal{L}(\sigma_{lp})$, respectively. Lastly, a uniformly distributed Z between variables a_u and b_u is represented as $Z \sim \mathcal{U}(a_u, b_u)$. \sim is used to indicate “has the distribution of”.

The rest of the paper is organized as follows. Section II describes the channel and system model of mmWave massive MIMO systems. Section III elaborates the proposed work and

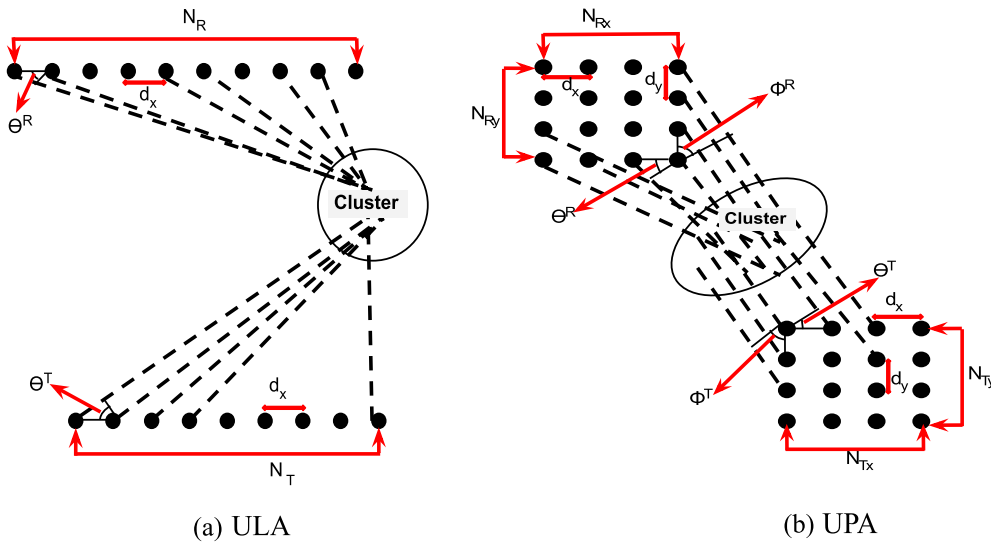


FIGURE 1. Beamforming between transmitter and receiver with different antenna configurations

also provides the algorithmic steps of the proposed method. Section IV discusses the simulation results, and finally, Section V concludes the paper.

II. CHANNEL AND SYSTEM MODEL

A. CHANNEL MODEL

Consider a mmWave massive MIMO channel with N_T transmit and N_R receive antennas. The geometrical model of $\mathbf{H} \in \mathbb{C}^{N_R \times N_T}$ is given in [11], [23] as:

$$\mathbf{H} = \sqrt{\frac{N_R N_T}{\rho}} \sum_{l=1}^L \alpha_l \mathbf{A}_T(l) \mathbf{A}_R(l)^H, \quad (1)$$

where $\mathbf{A}_T(l) \in \mathbb{C}^{N_T \times 1}$ and $\mathbf{A}_R(l) \in \mathbb{C}^{N_R \times 1}$ represent the steering vectors at the transmitter and receiver of the l^{th} path, respectively. In addition, L is the total number of dominant paths. The maximum possible value of L can be obtained using $L = \sum_{j=1}^{N_c} L_j$, where N_c is the total number of clusters and L_j is the number of dominant paths in the j^{th} cluster. Furthermore, α_l is the complex small scale fading gain of the l^{th} path and ρ is the average path loss between transmitter and receiver. The channel model of (1) can be re-written in the matrix form as:

$$\mathbf{H} = \mathbf{A}_R \mathbf{Z} \mathbf{A}_T^H, \quad (2)$$

where $\mathbf{A}_R \in \mathbb{C}^{N_R \times L}$ and $\mathbf{A}_T \in \mathbb{C}^{N_T \times L}$ are given by $[\mathbf{A}_R(1) \ \mathbf{A}_R(2) \ \dots \ \mathbf{A}_R(L)]$ and $[\mathbf{A}_T(1) \ \mathbf{A}_T(2) \ \dots \ \mathbf{A}_T(L)]$, respectively. $\mathbf{Z} \in \mathbb{C}^{L \times L}$ is a diagonal matrix with diagonal entries $\sqrt{\frac{N_T N_R}{\rho}} \alpha_l$, where $l = 1, 2, \dots, L$.

Based upon the geometrical arrangement of the antennas at the transmitter as well as the receiver, different type of steering vectors can be obtained [21]. The commonly used geometrical arrangements are uniform linear array (ULA) and uniform planar array (UPA), which are described below.

1) ULA

For ULA, antennas are placed in a line with uniform spacing of d_x between all consecutive antennas as shown in Fig. 1. If Θ_l^T is the azimuth angle of departure (AoD) of the l^{th} path, then the steering vector at the transmitter for the l^{th} path will be given by

$$\mathbf{A}_T(l) = \frac{1}{\sqrt{N_T}} \left[1 e^{j \frac{2\pi}{\lambda_c} d_x \sin \Theta_l^T} \dots \dots e^{j \frac{2\pi}{\lambda_c} d_x (N_T - 1) \sin \Theta_l^T} \right]^T. \quad (3)$$

Similarly the steering vector of ULA at the receiver for the l^{th} path can be obtained from (3) by replacing AoD, i.e., Θ_l^T with angle of arrival (AoA), i.e., Θ_l^R and N_T with N_R . Further, λ_c is the wavelength of the signal. Moreover, inline with the previous work [20], [21], it is assumed that AoA and AoD lie on the discretized grids.

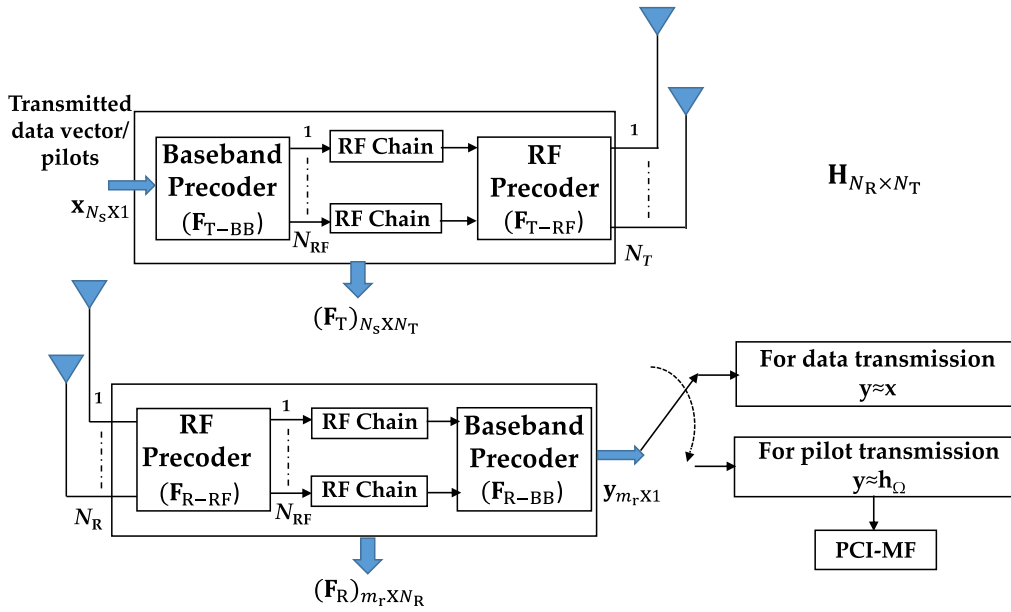
From (2) and (3), it is observed that the structure of \mathbf{A}_T and \mathbf{A}_R for ULA resemble normalized DFT matrix and hence, the DFT matrix can be segregated from (2) as follows

$$\begin{aligned} \mathbf{H} &= \mathcal{D}_{N_R} \mathcal{D}_{N_R}^H \mathbf{A}_R \mathbf{Z} \mathbf{A}_T^H \mathcal{D}_{N_T} \mathcal{D}_{N_T}^H \\ &= \mathcal{D}_{N_R} \mathbf{S} \mathcal{D}_{N_T}^H, \end{aligned} \quad (4)$$

where $\mathbf{S} = \mathcal{D}_{N_R}^H \mathbf{A}_R \mathbf{Z} \mathbf{A}_T^H \mathcal{D}_{N_T} \in \mathbb{C}^{N_R \times N_T}$ is a diagonal matrix with L non-zero diagonal entries and contains the information of AoAs, AoDs and α_l .

2) UPA

For UPA, antennas are placed in a plane, with d_x and d_y spacing between two consecutive antennas lying in horizontal and vertical line, respectively as shown in Fig. 1. Let us assume that N_{Tx} and N_{Ty} are the number of antennas placed horizontally and vertically, respectively, at the transmitter such that $N_T = N_{Tx} N_{Ty}$. Similarly, N_{Rx} and N_{Ry} are the number of antennas placed horizontally and vertically, respectively, at


FIGURE 2. System model.

the receiver such that $N_R = N_{R_x} N_{R_y}$. If Θ_l^T and Φ_l^T are the azimuth and elevation AoDs of the l^{th} path, respectively, then the steering vector at the transmitter for UPA will be given by

$$\mathbf{A}_T(l) = \frac{1}{\sqrt{N_{T_x} N_{T_y}}} \left[1 \ e^{j \frac{2\pi}{\lambda c} [d_x \sin \Theta_l^T \cos \Phi_l^T + d_y \sin \Theta_l^T \sin \Phi_l^T]} \ \dots \dots \right. \\ \left. e^{j \frac{2\pi}{\lambda c} [d_x (N_{T_x} - 1) \sin \Theta_l^T \cos \Phi_l^T + d_y (N_{T_y} - 1) \sin \Theta_l^T \sin \Phi_l^T]} \right]^T. \quad (5)$$

Similarly, the steering vector of UPA at the receiver for the l^{th} path can be obtained from (5) by replacing Θ_l^T with Θ_l^R , Φ_l^T with Φ_l^R (elevation AoA), N_{T_x} with N_{R_x} and, N_{T_y} with N_{R_y} .

Unlike ULA, in UPA the structure of \mathbf{A}_T and \mathbf{A}_R resemble the Kronecker product of the normalized DFT matrices (from (2), (5)) and hence, (2) can be simplified as below:

$$\mathbf{H} = \mathcal{K}_{N_R} \mathcal{K}_{N_R}^H \mathbf{K}_R \mathbf{Z} \mathbf{K}_T^H \mathcal{K}_{N_T} \mathcal{K}_{N_T}^H \\ = \mathcal{K}_{N_R} \mathbf{S} \mathcal{K}_{N_T}^H, \quad (6)$$

where $\mathcal{K}_{N_R} = \mathcal{D}_{N_{R_x}} \otimes \mathcal{D}_{N_{R_y}}$ and $\mathcal{K}_{N_T} = \mathcal{D}_{N_{T_x}} \otimes \mathcal{D}_{N_{T_y}}$. Further, $\mathbf{S} = \mathcal{K}_{N_R}^H \mathbf{A}_R \mathbf{Z} \mathbf{A}_T^H \mathcal{K}_{N_T} \in \mathbb{C}^{N_R \times N_T}$ is a diagonal matrix with L non-zero diagonal entries containing the information of AoAs, AoDs (azimuth as well as elevation), and α_l .

From (4) and (6), it is observed that $\mathbf{S} \in \mathbb{C}^{N_R \times N_T}$ has only L non-zero diagonal coefficients. This implies that \mathbf{S} is a sparse matrix because the number of non-zero coefficients is much smaller than the total number of coefficients in the matrix i.e., $L \ll N_T N_R$. Furthermore, it is a diagonal matrix with the number of non-zero coefficients at the diagonal less than their dimension ($L < \min(N_T, N_R)$). Hence, \mathbf{H} is a low-rank matrix.

In mmWave massive MIMO systems, the value of N_R and N_T is large and hence, the estimation of many channel coefficients corresponding to \mathbf{H} will be impractical. Therefore, in Section-III, various properties of massive MIMO based mmWave channel matrix, such as low rank property, sparsity and its DFT representation have been utilized jointly to recover entire CSI from a few estimated channel coefficients.

B. SYSTEM MODEL

Given a hybrid architecture of mmWave massive MIMO system with N_{RF} number of RF chains deployed at both transmitter as well as receiver. Let us assume that the transmitter is beamforming a data stream of length N_s , represented by \mathbf{x} at the receiver (shown in Fig. 2). The transmitter applies an $N_{RF} \times N_s$ baseband precoder denoted by \mathbf{F}_{T-BB} , followed by an $N_T \times N_{RF}$ RF precoder denoted by \mathbf{F}_{T-RF} and hence, the transmitter precoding matrix is given by $\mathbf{F}_T = \mathbf{F}_{T-RF} \times \mathbf{F}_{T-BB}$. The signal observed at the receiver is passed to an $N_{RF} \times N_R$ RF precoder denoted by \mathbf{F}_{R-RF} , followed by an $m_r \times N_{RF}$ baseband precoder to obtain m_r measurements denoted by \mathbf{F}_{R-BB} and hence, the receiver combining precoding matrix is given by $\mathbf{F}_R = \mathbf{F}_{R-BB} \times \mathbf{F}_{R-RF}$. The system model has been illustrated in Fig. 2.

1) TRAINING PHASE

During the training phase, the transmitter transmits the known data symbol, also known as pilot to estimate the channel coefficients. If the transmitter is beamforming a pilot p , i.e., $N_s = 1$, then the combined received signal at the receiver with m_r measurements of p can be written as

$$\mathbf{y} = \mathbf{F}_R \mathbf{H} \mathbf{F}_T p + \mathbf{n}, \quad (7)$$

where $\mathbf{F}_T \in \mathbb{C}^{N_T \times 1}$. Further, the receiver combining precoding matrix obtaining m_r measurements of the transmitted symbol at the receiver can be expressed as $\mathbf{F}_R = [\mathbf{f}_{R_1} \mathbf{f}_{R_2} \dots \mathbf{f}_{R_{m_r}}]' \in \mathbb{C}^{m_r \times N_R}$, where $\mathbf{f}_{R_i} \in \mathbb{C}^{N_R \times 1} \forall i$. Additionally, $\mathbf{n} \in \mathbb{C}^{m_r \times 1}$ is the noise vector and $\mathbf{H} \in \mathbb{C}^{N_R \times N_T}$ is the mmWave MIMO channel matrix.

It may be noted that inline with the previous work [21], [24], [27], to reduce the power consumption and complexity during the training phase, only one transmitting antenna is activated in each transmission. Hence, the number of pilots transmitted is equal to the number of transmitting antennas selected. If i^{th} transmitting antenna is activated, then \mathbf{F}_T should be designed in such a way that $\mathbf{F}_T(i) = 1$ and all the remaining entries will be zero [24]. The pilot, p is known at the receiver and assumed to be 1. Let's assume, $H(i, j_1)$, $H(i, j_2)$ and $H(i, j_3)$ needs to be estimated, which implies $\mathbf{f}_{R_1}(j_1) = 1$, $\mathbf{f}_{R_2}(j_2) = 1$, $\mathbf{f}_{R_3}(j_3) = 1$, and all the remaining entries of \mathbf{F}_R will be zero and hence, the received signal, $\mathbf{y} = [H(i, j_1)H(i, j_2)H(i, j_3)]'$. It may be noted that the number of channels estimated per transmission is limited by m_r , which is again limited by the number of RF chains at the receiver (N_{RF}), as $m_r \leq N_{RF}$. Therefore, in order to reduce the pilots overhead and hardware constraints during the training phase, only M coefficients of \mathbf{H} have been estimated from the total $N_T N_R$ coefficients. In the subsequent section, we will show how the complete channel matrix can be estimated from these M coefficients.

III. PROPOSED METHOD: PCI-MF

This section contains the proposed *PCI-MF* method, which recovers the entire channel matrix from a few estimated channel coefficients (i.e., M). The estimated coefficients of \mathbf{H} are stacked in a vector $\mathbf{h}_\Omega \in \mathbb{C}^{M \times 1}$ and is written as:

$$\mathbf{h}_\Omega = \Phi \mathbf{h} + \mathbf{n}, \quad (8)$$

$\mathbf{h} \in \mathbb{C}^{N_R N_T \times 1}$ is equal of $\mathbf{H}(\cdot)$ and $\mathbf{n} \in \mathbb{C}^{N_R N_T \times 1}$ is a complex Gaussian noise vector. However, the matrix $\Phi \in \mathbb{B}^{M \times N_R N_T}$ is a measurement matrix and is known as the partial canonical identity (PCI) matrix. We illustrate the above with an example. Consider a channel matrix, $\mathbf{H} = \begin{bmatrix} h_{11} & h_{12} \\ h_{21} & h_{22} \end{bmatrix}$, and only two coefficients h_{21} and h_{22} have been estimated in the training phase. Hence, $\mathbf{h}_\Omega = [h_{21} \ h_{22}]'$ and the corresponding PCI matrix, Φ will be $\begin{bmatrix} 0 & 0 & 1 & 0 \\ 0 & 0 & 0 & 1 \end{bmatrix}$.

For ULA, using (4), $\mathbf{h} = (\mathcal{D}_{NT}^* \otimes \mathcal{D}_{NR})\mathbf{s}$, where $\mathbf{s} = \mathbf{S}(\cdot)$. Hence, (8) can also be re-written as:

$$\begin{aligned} \mathbf{h}_\Omega &= \Phi (\mathcal{D}_{NT}^* \otimes \mathcal{D}_{NR})\mathbf{s} + \mathbf{n} \\ &= \Phi \Psi_l \mathbf{s} + \mathbf{n} \quad (\because \Psi_l = \mathcal{D}_{NT}^* \otimes \mathcal{D}_{NR}) \\ &= \mathbf{A}_l \mathbf{s} + \mathbf{n} \quad (\because \mathbf{A}_l = \Phi \Psi_l), \end{aligned} \quad (9)$$

where $\mathbf{A}_l \in \mathbb{C}^{M \times N_T N_R}$ and $\Psi_l \in \mathbb{C}^{N_T N_R \times N_T N_R}$. However, for UPA (from (6)) $\mathbf{h} = (\mathcal{K}_{NT}^* \otimes \mathcal{K}_{NR})\mathbf{s}$, where $\mathbf{s} = \mathbf{S}(\cdot)$. Hence, (8) can be re-written as

$$\begin{aligned} \mathbf{h}_\Omega &= \Phi (\mathcal{K}_{NT}^* \otimes \mathcal{K}_{NR})\mathbf{s} + \mathbf{n} \\ &= \Phi ((\mathcal{D}_{NT_x} \otimes \mathcal{D}_{NT_y})^* \otimes (\mathcal{D}_{NR_x} \otimes \mathcal{D}_{NR_y}))\mathbf{s} + \mathbf{n} \end{aligned}$$

$$\begin{aligned} &= \Phi \Psi_p \mathbf{s} + \mathbf{n} \\ &= \mathbf{A}_p \mathbf{s} + \mathbf{n} \quad (\because \mathbf{A}_p = \Phi \Psi_p), \end{aligned} \quad (10)$$

where $\mathbf{A}_p \in \mathbb{C}^{M \times N_T N_R}$ and $\Psi_p \in \mathbb{C}^{N_T N_R \times N_T N_R}$.

Since $\mathbf{s} \in \mathbb{C}^{N_T N_R \times 1}$ is the sparse vector, (9) and (10) resemble the compressive sensing framework [28], where \mathbf{h}_Ω is the compressive measurements, Φ is the sensing/ measurement matrix, and Ψ_l and Ψ_p are the sparsifying matrices. According to the theory of CS, the sparse vector \mathbf{s} can be recovered perfectly from \mathbf{h}_Ω , if mutual incoherence property is satisfied by matrices (Φ, Ψ_l) and (Φ, Ψ_p) , respectively [28].

The *mutual incoherence property* is said to be satisfied by two matrices, if they are incoherent. The coherence between matrices, say \mathbf{Q} and \mathbf{P} of size $M \times N$ and $N \times N$, respectively, is calculated as

$$\mu_c(\mathbf{Q}, \mathbf{P}) = \sqrt{N} \max_{\forall i, j} |(\mathbf{Q}_i, \mathbf{P}_j)|, \quad (11)$$

where \mathbf{Q}_i and \mathbf{P}_j represents i^{th} and j^{th} column of orthonormal matrix \mathbf{Q}^T and \mathbf{P} , respectively. The range of $\mu_c(\mathbf{Q}, \mathbf{P}) \in [1, \sqrt{N}]$. Here, $\mu_c = 1$ represents maximum incoherence between the matrices. If one of the matrices is Φ , i.e., PCI matrix, the coherence expression will reduce to [29], [30]

$$\mu_c(\Phi, \mathbf{P}) = \sqrt{N} \max_{\forall i, j} |\mathbf{P}(i, j)|. \quad (12)$$

Therefore, the mutual coherence between Φ and Ψ_l for CS framework shown in (9) is calculated using (12) as follows:

$$\mu_c(\Phi, \Psi_l) = \sqrt{N_T N_R} \max_{\forall i, j} |\Psi_l(i, j)| = 1. \quad (13)$$

Similarly, the mutual coherence between Φ and Ψ_p for CS framework shown in (10) will be given by:

$$\mu_c(\Phi, \Psi_p) = \sqrt{N_T N_T N_R N_R} \max_{\forall i, j} |\Psi_p(i, j)| = 1. \quad (14)$$

From (13) and (14), it is observed that both ULA (9) as well as UPA (10) CS frameworks have minimum coherence of 1 and hence, the following l^1 minimization problem has been solved to recover \mathbf{s} from \mathbf{h}_Ω :

$$P_1 : \min_s \|\mathbf{h}_\Omega - \mathbf{A}\mathbf{s}\|_2^2 + \lambda \|\mathbf{s}\|_1, \quad (15)$$

where $\mathbf{A} = \begin{cases} \mathbf{A}_l & \text{for ULA} \\ \mathbf{A}_p & \text{for UPA} \end{cases}$, and λ is the regularization parameters to control the level of sparsity and the data accuracy. Iterative soft thresholding method (ISTA) [31], [32] can be used to solve (15). The sparse vectors \mathbf{s} determined above either for ULA or for UPA can be used to estimate channel matrix \mathbf{H} by jointly exploiting its low-rank nature in a matrix factorization framework as follows:

$$\begin{aligned} P_2 : \min_{\mathbf{H}, \mathbf{U}, \mathbf{V}} & (\|\mathbf{H} - \mathbf{U}\mathbf{V}\|_F^2 + \rho_1 \|\mathbf{U}\|_F^2 \\ & + \rho_2 \|\mathbf{V}\|_F^2) + \mu \|\mathbf{h}_\Omega - \mathbf{A}\mathbf{s}\|_F^2. \end{aligned} \quad (16)$$

Matrices \mathbf{U} and \mathbf{V} have the dimension of $N_R \times r$ and $r \times N_T$, respectively, where r is the rank of the channel matrix \mathbf{H} that can be determined by calculating the number of non-zero

values in \mathbf{s} .¹ The parameter ρ_1 and ρ_2 control the magnitude of matrices \mathbf{U} and \mathbf{V} , respectively. The term $\mu\|\mathbf{h}_\Omega - \mathbf{A}\mathbf{s}\|_F^2$ has been added to penalize the error caused due to noisy estimation of \mathbf{s} (in (15)). Generally, \mathbf{s} will be estimated noisy for lower received signal-to-noise ratio (SNR) and/or for low value of measurement ratio defined as $\text{MR} = \frac{M}{N_T N_R}$. Hence, addition of this term provides robust estimation of \mathbf{H} . A higher value of μ implies more weight to the term $\mu\|\mathbf{h}_\Omega - \mathbf{A}\mathbf{s}\|_F^2$, in the case of noisy estimation of \mathbf{s} . The problem P_2 given in (16) can be solved using the alternate direction method of multipliers (ADMM) by dividing into following three sub-problems [33] as follows:

$$P_2(a) : \min_{\mathbf{U}} \|\mathbf{H} - \mathbf{U}\mathbf{V}\|_F^2 + \rho_1 \|\mathbf{U}\|_F^2. \quad (17)$$

$$P_2(b) : \min_{\mathbf{V}} \|\mathbf{H} - \mathbf{U}\mathbf{V}\|_F^2 + \rho_2 \|\mathbf{V}\|_F^2. \quad (18)$$

$$P_2(c) : \min_{\mathbf{H}} \|\mathbf{H} - \mathbf{U}\mathbf{V}\|_F^2 + \mu\|\mathbf{h}_\Omega - \mathbf{A}\mathbf{s}\|_F^2. \quad (19)$$

All three sub-problems mentioned above are the simple least square problems and are solved as follows. The problem $P_2(a)$ is written as:

$$P_2(a) : \min_{\mathbf{U}} \|\tilde{\mathbf{H}} - \mathbf{U}\tilde{\mathbf{V}}\|_F^2, \quad (20)$$

where $\tilde{\mathbf{H}} = [\mathbf{H} \quad \mathbf{0}_{N_R \times r}]$ and $\tilde{\mathbf{V}} = [\mathbf{V} \quad \sqrt{\rho_1}\mathbf{I}_r]$. This implies

$$\mathbf{U} = \tilde{\mathbf{H}}\tilde{\mathbf{V}}'(\tilde{\mathbf{V}}\tilde{\mathbf{V}}')^{-1}. \quad (21)$$

Similarly the problem $P_2(b)$ is written as:

$$P_2(b) : \min_{\mathbf{V}} \|\hat{\mathbf{H}} - \hat{\mathbf{U}}\mathbf{V}\|_F^2, \quad (22)$$

where $\hat{\mathbf{H}} = \begin{bmatrix} \mathbf{H} \\ \mathbf{0}_{r \times N_T} \end{bmatrix}$ and $\hat{\mathbf{U}} = \begin{bmatrix} \mathbf{U} \\ \sqrt{\rho_2}\mathbf{I}_r \end{bmatrix}$. Hence,

$$\mathbf{V} = (\hat{\mathbf{U}}'\hat{\mathbf{U}})^{-1}\hat{\mathbf{U}}'\hat{\mathbf{H}}. \quad (23)$$

The problem $P_2(c)$ is written as:

$$\min_{\mathbf{h}} \|\mathbf{h} - (\mathbf{I}_{N_T} \otimes \mathbf{U})\mathbf{v}\|_F^2 + \mu\|\Phi\mathbf{h} - \mathbf{A}\mathbf{s}\|_F^2, \quad (24)$$

where $\mathbf{h} = \mathbf{H}(\cdot)$ and $\mathbf{v} = \mathbf{V}(\cdot)$. Differentiating (24) for \mathbf{h} yields:

$$\mathbf{h} = (\mathbf{I}_{N_T N_R} + \mu\Phi'\Phi)^{-1}((\mathbf{I}_{N_T} \otimes \mathbf{U})\mathbf{v} + \mu\Phi'\mathbf{A}\mathbf{s}). \quad (25)$$

It is to be noted that for high received SNR with high MR,² the problem $P_2(c)$ can be simply reduced into two steps: 1) $\mathbf{H} = \mathbf{U}\mathbf{V}$. 2) Replace the estimated channel coefficients i.e., \mathbf{h}_Ω by $\mathbf{A}\mathbf{s}$. The algorithmic steps for the proposed PCI-MF method are provided in Algorithm 1. For better understanding,

¹The coefficients of \mathbf{s} having smaller value tending towards zero will be considered as zero.

²Typically, for our experimental setup, low SNR implies 0 to 5 dB and low MR implies availability of 10% to 20% channel coefficients. Hence, high SNR with high MR implies availability of more than 5 dB SNR and 20% channel coefficients.

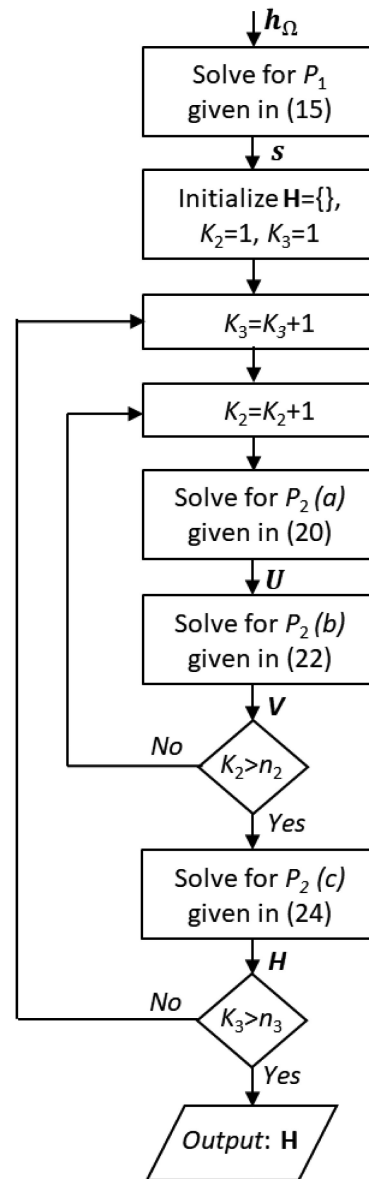


FIGURE 3. Flow diagram of the PCI-MF algorithm.

a flow diagram of the proposed algorithm is also provided in Fig. 3.

IV. COMPLEXITY ANALYSIS

The complexity of the state-of-the-art methods such as for the two-stage methods of [20] and [21] is given as $\mathcal{O}(\max(N_R, N_T)N_R N_T)$ because both these methods are dominated by singular value thresholding (SVT) [22].

The complexity of the proposed method will depend upon the complexity of problem P_1 and $P_2(a) - (c)$. The complexity of P_1 , which is usually solved by method such as ISTA is given as $\mathcal{O}(MN_R N_T)$. However, the complexity of $P_2(a)$ and $P_2(b)$ is $\mathcal{O}(rN_R N_T)$. For high SNR with high MR, the complexity of $P_2(c)$ is also $\mathcal{O}(rN_R N_T)$. Therefore, in this case,

Algorithm 1: PCI-MF.

Input: $\Phi, \mathbf{h}_\Omega, N_T, N_R, N_{Tx}, N_{Ty}, N_{Rx}, N_{Ry}, \mu, \lambda, \rho_1, \rho_2, n_1, n_2, n_3^3$

Initialization: $\mathbf{s} = \text{zeros}(N_T N_R \times 1)$

For ULA: $\Psi_l = \mathcal{D}_{NT}^* \otimes \mathcal{D}_{NR}^4$

For UPA: $\Psi_p = (\mathcal{D}_{N_{Tx}} \otimes \mathcal{D}_{N_{Ty}})^* \otimes (\mathcal{D}_{N_{Rx}} \otimes \mathcal{D}_{N_{Ry}})$

$\mathbf{A} = \Psi\Phi$, where $\Psi = \begin{cases} \Psi_l & \text{for ULA} \\ \Psi_p & \text{for UPA} \end{cases}$

$\alpha = \max(\text{eig}(\mathbf{A}'\mathbf{A}))$

for $k_1 = 1 : n_1$ **do**

$\mathbf{s} = \text{sgn}(\mathbf{s} + \frac{1}{\alpha}\mathbf{A}'\mathbf{h}_\Omega - \mathbf{A}\mathbf{s}) \max(0, |\mathbf{A}'\mathbf{h}_\Omega - \mathbf{A}\mathbf{s}| - \frac{\lambda}{2\alpha})^5$

end for

$r = \text{sparsity of } \mathbf{s}$

$\mathbf{h} = \Psi\mathbf{s}$

for $k_2 = 1 : n_2$ **do**

$\mathbf{H} = \text{resize}(\mathbf{h}, [N_R, N_T])^6$

$\mathbf{V} = \mathbf{H}(1 : r, :)$

for $k_3 = 1 : n_3$ **do**

$\tilde{\mathbf{H}} = [\mathbf{H} \quad \mathbf{0}_{N_R \times r}]$ and $\tilde{\mathbf{V}} = [\mathbf{V} \quad \sqrt{\rho_1}\mathbf{I}_r]$

$\mathbf{U} = \tilde{\mathbf{H}}\tilde{\mathbf{V}}'(\tilde{\mathbf{V}}\tilde{\mathbf{V}}')^{-1}$

$\hat{\mathbf{H}} = \begin{bmatrix} \mathbf{H} \\ \mathbf{0}_{r \times N_T} \end{bmatrix}, \hat{\mathbf{U}} = \begin{bmatrix} \mathbf{U} \\ \sqrt{\rho_2}\mathbf{I}_r \end{bmatrix}$

$\mathbf{v} = (\hat{\mathbf{U}}'\hat{\mathbf{U}})^{-1}\hat{\mathbf{U}}'\hat{\mathbf{H}}$

end for

At low SNR and/or low MR:

$\mathbf{h} = (\mathbf{I}_{N_T N_R} + \mu\Phi'\Phi)^{-1}(\mathbf{I}_{N_T} \otimes \mathbf{U})\mathbf{v} + \mu\Phi'\mathbf{A}\mathbf{s}$

At high SNR with high MR:

$\mathbf{H} = \mathbf{U}\mathbf{V}$

$\mathbf{p} = \text{find}(\Phi(:, :)) == 1$

$\mathbf{h} = \mathbf{H}(:, \mathbf{p}), \mathbf{h}(\mathbf{p}) = \mathbf{A}\mathbf{s}$

end for

$\mathbf{H} = \text{resize}(\mathbf{h}, [N_R, N_T])$

Output: \mathbf{H}

the complexity of PCI-MF is $(\mathcal{O}(MN_R N_T + 3rN_R N_T)) \approx \mathcal{O}(MN_R N_T)$. The value of M varies from 1 to $N_R N_T$ and hence, the computational complexity of PCI-MF increases at higher values of M . Further, it is observed that the complexity of PCI-MF is dominated by ISTA and hence, method such as fast iterative soft thresholding method (FISTA) [32] can be used instead of ISTA to reduce the computational complexity of PCI-MF. However, at low SNR and/or low MR, the complexity of $P_2(c)$ is $(\mathcal{O}(N_R^2 N_T^2))$. Hence, the complexity of PCI-MF will be $(\mathcal{O}(MN_R N_T + 2rN_R N_T + N_R^2 N_T^2)) \approx \mathcal{O}(N_R^2 N_T^2)$, which is a trade-off between complexity and performance. It may be noted that the above is a rare scenario and is applicable for applications with the very low value of $\text{SNR} \leq 5$ dB

³ n_1, n_2 and n_3 represent the maximum number of iterations.

⁴ \mathcal{D}_a will generate a DFT matrix of size a .

⁵ $\text{sgn} = \begin{cases} -1 & \text{if } x < 0 \\ 0 & \text{if } x = 0 \\ 1 & \text{if } x > 0 \end{cases}$

⁶resize converts the given vector into a matrix of given size.

TABLE 1. Complexity Comparison

Algorithm	Complexity
LMaFit [34]	$\mathcal{O}(rN_R N_T)$
Two stage [20]	$\mathcal{O}(\max(N_R, N_T)N_R N_T)$
E. Vlachos et al. [21]	$\mathcal{O}(\max(N_R, N_T)N_R N_T)$
PCI-MF : At low SNR (≤ 5 dB) and/or low MR ($\leq 20\%$)	$\mathcal{O}(N_R^2 N_T^2)$
PCI-MF : At high SNR (>5 dB) with high MR ($>20\%$)	$\mathcal{O}(MN_R N_T)$

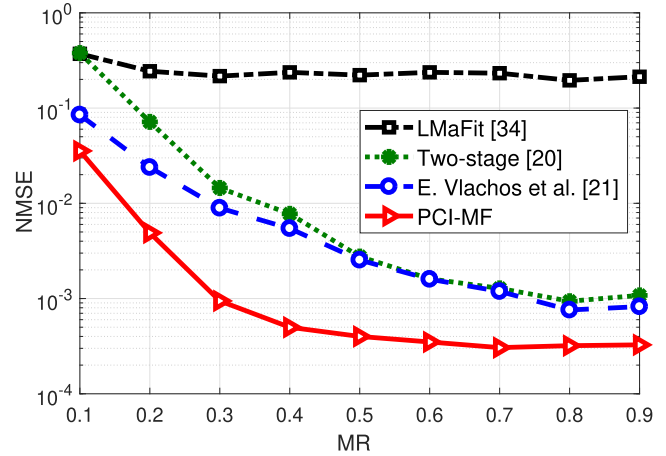


FIGURE 4. NMSE vs MR for ULA at 25 dB SNR with 32×32 MIMO configuration.

and also the very low percentage of $\text{MR} \leq 20\%$. Consider Table 1 that presents the complexity comparison of different algorithms.

V. SIMULATION AND DISCUSSION

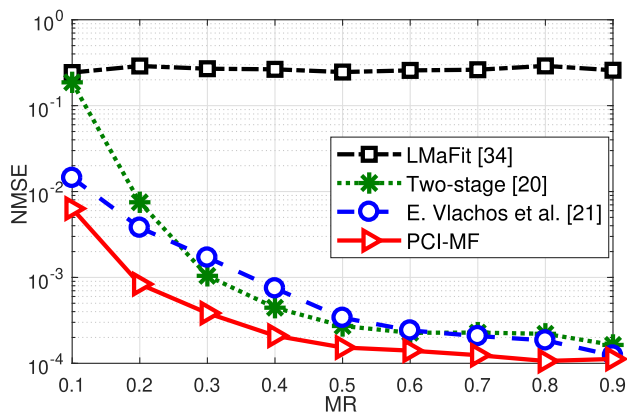
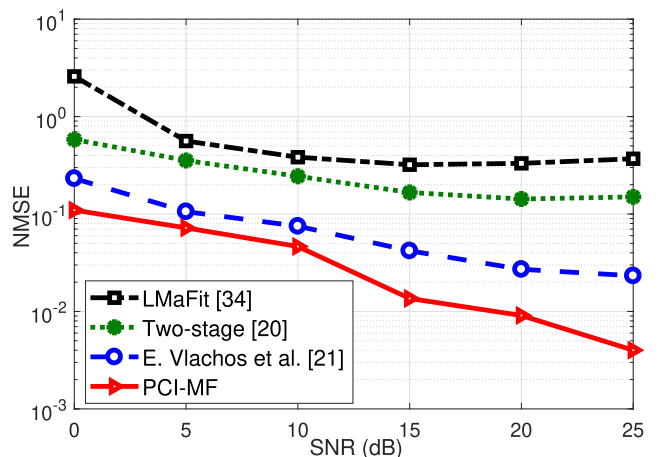
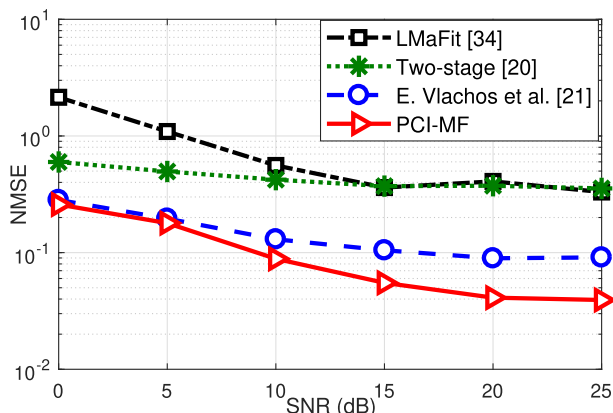
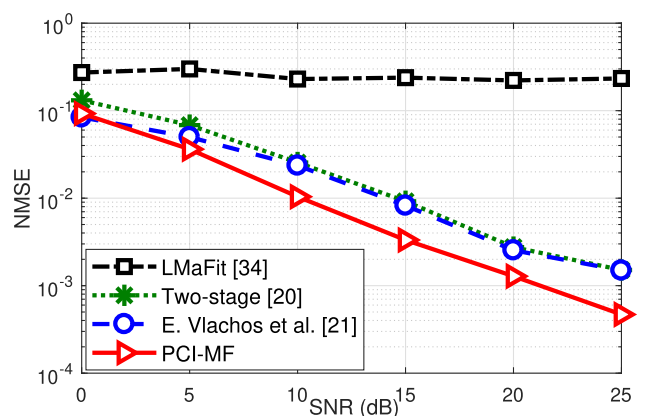
This section presents the simulation results of the proposed PCI-MF method. Results have been compared with the state-of-the-art methods such as the two-stage methods [20] and [21] presented by Xingjian *et al.* and by E. Vlachos *et al.* respectively. In addition to the above, the performance of PCI-MF has also been compared with the conventional matrix completion algorithm based on MF such as the low-rank matrix fitting (LMaFit) [34].

Simulations are performed against various parameters such as the MIMO configurations, SNR, MR, and L . Moreover, results have been obtained for two different operating frequencies (f_c) i.e., 90 GHz [21] and 28 GHz [25], [26]. The value of various parameters considered for both frequencies is summarized in Table 2. Furthermore, for 28 GHz, simulations are performed for real-world parameters obtained at New York City. It is to be noted that for all the simulations, the distance between two consecutive antennas placed either horizontally or vertically is $\frac{\lambda_c}{2}$, which implies $d_x = d_y = \frac{\lambda_c}{2}$. The value of the regularization parameters $\rho_1 = \rho_2 = 0.01$, whereas μ varies from 0.1 to 0.01.

For 90 GHz (Fig. 4–14), both AoA and AoD are Laplacian distributed with standard deviation 50° [21]. The value taken for the number of clusters (N_c) and the number of dominant paths in each cluster (L_k) are 2 and 1, respectively, which

TABLE 2. Simulation Parameters

f_c (GHz)	N_c	L_k	AoA/AoD	α_l
90 [21]	1	2	$\mathcal{L}(50^\circ)$	a) $\mathcal{R}(1)$ b) $\mathcal{NG}(0.5, 1)$
28 [25], [26]	$\max(1, \mathcal{P}(1.8))$	2	$\mathcal{N}(\mathcal{U}(0, 2\pi), \varepsilon(\lambda_a))$	$\mathcal{R}(\gamma_l 10^{0.1PL})$
			$\lambda_a^{-1} = \begin{cases} 15.5 & \text{for } \Theta_1^R \\ 6 & \text{for } \Phi_1^R \\ 10.2 & \text{for } \Theta_1^T \\ 0 & \text{for } \Phi_1^T \end{cases}$	$\gamma_l = \frac{\gamma'_l}{\sum_{i=1}^L \gamma'_i}$, $\gamma'_l = U_l^{r_\tau} 10^{-0.1Z_l}$, $U_l \sim \mathcal{U}(0, 1)$, $Z_l \sim \mathcal{N}(0, 16)$, $PL = \alpha + 10\beta \log_{10}(d) + \zeta$ dB, $\alpha = 72$, $\beta = 2.92$, $\zeta \sim \mathcal{N}(0, 8.7)$ dB), $d_{t-r} = 100$ m.


FIGURE 5. NMSE vs MR for ULA at 25 dB SNR with 64×64 MIMO configuration.

FIGURE 7. NMSE vs SNR for ULA at MR = 0.1 with 64×64 MIMO configuration.

FIGURE 6. NMSE vs SNR for ULA at MR = 0.1 with 32×32 MIMO configuration.

FIGURE 8. NMSE vs SNR for ULA at MR = 0.5 with 32×32 MIMO configuration.

implies $L = 2$. For Figs. 4–11 instantaneous path loss is Rayleigh distributed with unit variance [21] and antenna configuration is ULA. Results for UPA are shown in Fig. 13. In some previous works, it has been observed that Nakagami channel fading model fits better than the Rayleigh fading model for mmWave band, especially, with directional beamforming [35]–[37]. Therefore, results with Nakagami fading model are also shown in Fig. 14.

Figs. 4 and 5 compare the normalized mean square error (NMSE)⁷ against the measurement ratio (MR) for 32×32 and 64×64 MIMO configuration, respectively, with SNR = 25 dB. It is observed that PCI-MF outperforms all existing methods at all MR ratios and for both MIMO configurations. For instance, for 32×32 MIMO configuration at

⁷NMSE = $\frac{\|\mathbf{H} - \hat{\mathbf{H}}_e\|_F^2}{\|\mathbf{H}\|_F^2}$, where \mathbf{H} and $\hat{\mathbf{H}}_e$ are the actual and estimated channel matrices, respectively.

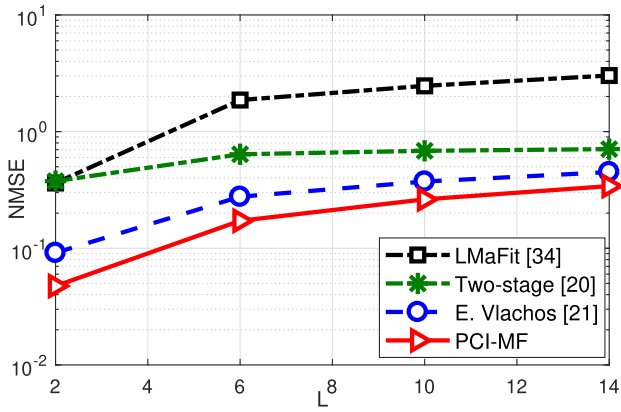


FIGURE 9. NMSE vs L for ULA at SNR = 25 dB, MR = 0.1 with 32×32 MIMO configuration.

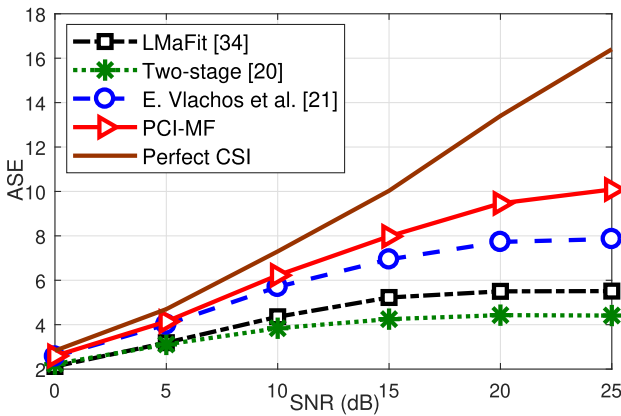


FIGURE 10. ASE vs SNR for ULA at MR = 0.1 with 32×32 MIMO configuration.

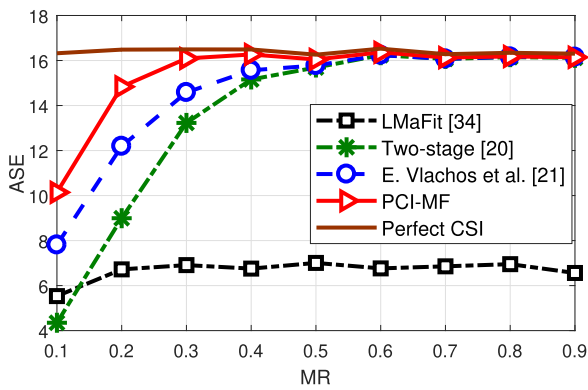


FIGURE 11. ASE vs MR for ULA at SNR = 25 dB with 32×32 MIMO configuration.

MR = 0.4, the state-of-the-art methods [20] and [21] yielded NMSE of 7.755×10^{-3} and 5.44×10^{-3} , respectively, as shown in Fig. 4. On the other hand, we obtained an NMSE of 0.499×10^{-3} using PCI-MF. Hence, an improvement of $10 \log_{10}(\frac{5.44 \times 10^{-3}}{0.499 \times 10^{-3}}) = 11.91$ dB and 10.375 dB is obtained as compared to [20] and [21], respectively. Similarly, an improvement of 3.22 dB and 5.52 dB is obtained for 64×64

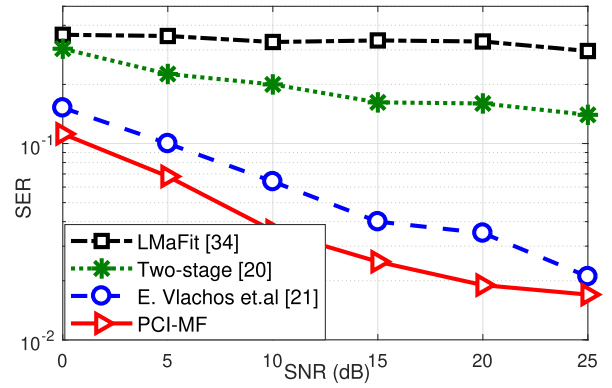


FIGURE 12. SER vs SNR for ULA at MR = 0.1 with 32×32 MIMO configuration.

MIMO configuration (Fig. 5) with PCI-MF compared to [20] and [21], respectively.

To show the robustness of PCI-MF, we computed NMSE against SNR with only 10% measurement ratio, i.e., MR = 0.1 in Figs. 6 and 7 for 32×32 and 64×64 MIMO configuration, respectively. It is observed that PCI-MF outperforms in all the above scenarios. To further validate the proposed work, NMSE is also shown against SNR at MR = 0.5 in Fig. 8.

In Fig. 9, NMSE is plotted against the number of paths, i.e., L for SNR = 25 dB and MR = 0.1 for 32×32 MIMO configuration. Results demonstrate that the performance of PCI-MF does not degrade even with different values of L .

It may be noted that the error between the estimated CSI and actual CSI will directly impact the achievable spectral efficiency (ASE) of the wireless system as shown below [21], [38]:

$$ASE = \log_2 \left| I_{N_R} + \frac{1}{N_T N_R (NMSE + \frac{1}{SNR})} \mathbf{H} \mathbf{H}^H \right| \quad (26)$$

bits/s/Hz.

Hence, in Fig. 10, the ASE is plotted against SNR at MR = 0.1 for 32×32 MIMO configuration. It is observed that at 25 dB SNR, [21] performs best among the existing methods and yields an ASE of 8 bits/sec/Hz. However, the proposed method PCI-MF obtains an ASE equal to 10 bits/sec/Hz. It is noted that the ASE obtained with perfect CSI is nearly 16 bits/sec/Hz. Therefore, in Fig. 11, we have plotted ASE by varying the MR and it is observed that at $MR \geq 0.3$, PCI-MF approaches close to the ASE value of 16 bits/sec/Hz, i.e., the value obtained with the perfect CSI.

Lastly, we examined the performance of the symbol error rate (SER) of PCI-MF against SNR by comparing it with other algorithms in Fig. 12. We modulated the data for ULA at MR = 0.1 with 32×32 MIMO configuration using BPSK (binary phase shift keying) modulation. The precoding vectors at the transmitter and receiver are implemented using random complex vectors in every iteration.

Fig. 13 shows the performance of PCI-MF with UPA. In this plot, NMSE is plotted against MR at 25 dB SNR for $64 \times$

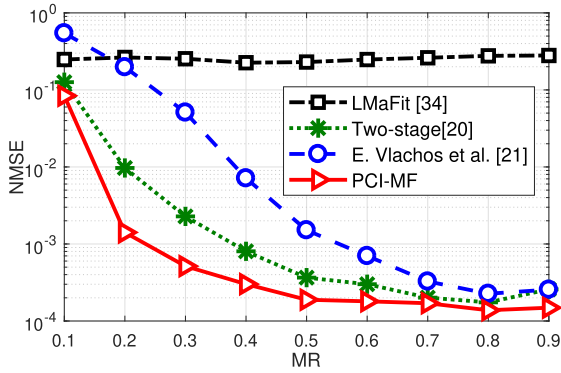


FIGURE 13. NMSE vs MR for UPA at SNR = 25 dB with 64 × 64 MIMO configuration.

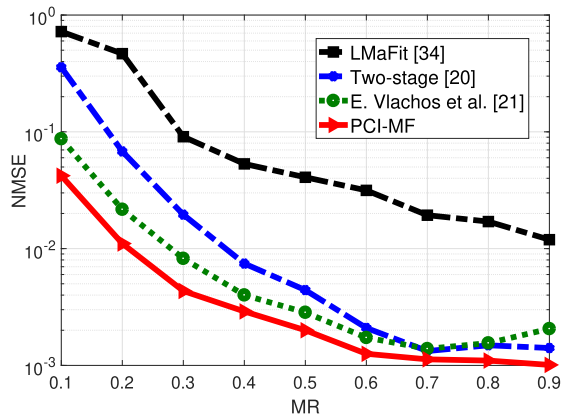


FIGURE 14. NMSE vs MR for ULA at SNR = 25 dB with 32 × 32 MIMO configuration in Nakagami fading with shape parameter as 0.5.

64 MIMO configuration, where $N_{T_x} = N_{T_y} = N_{R_x} = N_{R_y} = 16$. Therefore, it can be concluded that PCI-MF performs better for both ULA as well as UPA.

Fig. 14 evaluates the performance of PCI-MF in the presence of Nakagami fading channel. The shape parameter of Nakagami distribution (m) determines the fading channel conditions, for instance $m = 1$ represents Rayleigh fading and $m = 0.5$ represents half Gaussian pulse, which is severe than Rayleigh fading [39], [40]. Therefore, in Fig. 14, NMSE is plotted for $\mathcal{N}\mathcal{G}(0.5, 1)$ against MR at 25 dB SNR. From the plot, it is observed that PCI-MF performs good even with severe fading.

Fig. 15 shows the results for statistical parameter values derived from real world mmWave outdoor cellular propagation at 28 GHz collected in New York City [25], [26]. As per the collected data, the number of clusters are Poisson distributed with mean value equal to 1.8 and number of dominant paths in each cluster i.e., L_k is assumed to be 2. The AoA and AoD are Gaussian distributed with mean and variance equal to μ_a and σ_a^2 , respectively, where μ_a is uniformly distributed between 0 to 2π and σ_a is exponentially distributed with mean λ_a^{-1} . The values of λ_a^{-1} for azimuth AoA, elevation AoA, azimuth AoD and elevation AoD are 15.5, 6, 10.2 and 0, respectively [25], [26] (as summarized in Table 2). It considers a UPA with 64 × 64 MIMO configuration. The

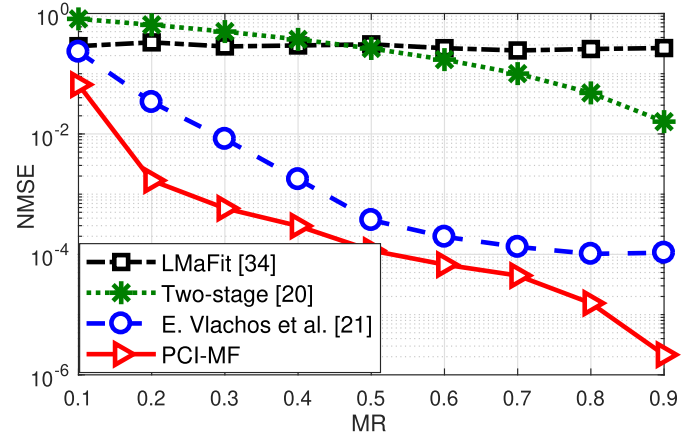


FIGURE 15. NMSE vs MR for realistic data set [25], [26] at SNR = 30 dB with $d = 100$ m.

instantaneous path loss is Rayleigh faded with σ_l^2 variance. The variance σ_l^2 for l^{th} path is given as $\sigma_l^2 = \gamma_l 10^{(0.1PL)}$, where $\gamma_l = \frac{\gamma'_l}{\sum_{i=1}^L \gamma'_i}$. Furthermore, $\gamma'_l = U_l^{r_\tau} 10^{-0.1Z_l}$, where r_τ is 2.8, $U_l \sim \mathcal{U}(0, 1)$ and $Z_l \sim \mathcal{N}(0, 16)$. Moreover, $PL = \alpha + 10\beta \log_{10}(d) + \zeta$ dB, where $\alpha = 72$, $\beta = 2.92$ and $\zeta \sim \mathcal{N}(0, 8.7$ dB) for non line-of-sight (NLOS) [25], [26]. The distance considered between transmitter and receiver (d_{t-r}) is 100 m. It is observed that for realistic data set the performance of all existing methods except [21] is not acceptable, since they hardly achieve an NMSE of 10^{-2} even when 90% data is available. However, NMSE achieved by [21] is 2.952×10^{-5} . Since PCI-MF achieves NMSE of 7.418×10^{-10} , 16.933 dB improvement is obtained as compared to [21].

VI. CONCLUSION

In this paper, a novel method PCI-MF has been proposed to recover the mmWave massive MIMO CSI from a few noisy channel coefficients. The performance of the method has been evaluated by calculating NMSE between the actual CSI and the recovered CSI. NMSE results show considerable improvement in performance with PCI-MF compared to the state-of-the-art methods. For validating the robustness of PCI-MF, the NMSE is simulated with various parameters, such as different MIMO configurations, low and high values of SNR and MR, as well as different channel fading models. It is observed that PCI-MF consistently outperforms in different MIMO configurations such as 32 × 32, 64 × 64, for all values of SNR and also for all MR. The improvement in performance is observed with both ULA as well as UPA antenna configurations. The performance of PCI-MF is also shown by evaluating SER and ASE. It is observed that PCI-MF outperforms the existing methods and approaches the ASE values of perfect CSI. For instance, at 25 dB SNR, ASE of 16.49 bits/sec/Hz is obtained with perfect CSI for 32 × 32 MIMO configuration. Using PCI-MF, with only 30% availability of channel information, ASE of 16.09 bits/sec/Hz (close to perfect CSI) has been obtained.

In order to validate the performance of PCI-MMF in realistic scenarios, another data set of New York City with real-world outdoor cellular propagation parameters has also been considered. It is observed that even in a practical scenario when transmitter and receiver are 100 m apart, PCI-MF obtains 5.45 dB and 16.933 dB improvement with 10% and 90% availability of channel information, respectively, as compared to the existing methods.

ACKNOWLEDGMENT

The authors would like to thank Visvesvaraya research fellowship, Department of Electronics and Information Technology, Ministry of Communication and IT, Government of India, for providing financial support for this work.

REFERENCES

- [1] A. Gupta and R. K. Jha, "A survey of 5G network: Architecture and emerging technologies," *IEEE Access*, vol. 3, pp. 1206–1232, 2015.
- [2] R. Baldemair *et al.*, "Evolving wireless communications: Addressing the challenges and expectations of the future," *IEEE Veh. Technol. Mag.*, vol. 8, no. 1, pp. 24–30, Mar. 2013.
- [3] J. G. Andrews *et al.*, "What will 5G be?," *IEEE J. Sel. Areas Commun.*, vol. 32, no. 6, pp. 1065–1082, 2014.
- [4] M. Agiwal, A. Roy, and N. Saxena, "Next generation 5G wireless networks: A comprehensive survey," *IEEE Commun. Surv. Tutorials*, vol. 18, no. 3, pp. 1617–1655, 2016.
- [5] T. S. Rappaport, J. N. Murdock, and F. Gutierrez, "State of the art in 60-ghz integrated circuits and systems for wireless communications," *Proc. IEEE*, vol. 99, no. 8, pp. 1390–1436, 2011.
- [6] S. Rangan, T. S. Rappaport, and E. Erkip, "Millimeter wave cellular wireless networks: Potentials and challenges," in *Proc. IEEE*, pp. 366–385, Mar. 2014, doi: [10.1109/JPROC.2014.2299397](https://doi.org/10.1109/JPROC.2014.2299397).
- [7] S. A. Busari, K. M. S. Huq, S. Mumtaz, L. Dai, and J. Rodriguez, "Millimeter-wave massive mimo communication for future wireless systems: A survey," *IEEE Commun. Surv. Tutorials*, vol. 20, no. 2, pp. 836–869, Secondquarter 2018.
- [8] J. Wang *et al.*, "Beam codebook based beamforming protocol for multi-gbps millimeter-wave WPAN systems," in *Proc. IEEE Global Telecommun. Conf.*, 2009, pp. 1–6.
- [9] S. Hur, T. Kim, D. J. Love, J. V. Krogmeier, T. A. Thomas, and A. Ghosh, "Millimeter wave beamforming for wireless backhaul and access in small cell networks," *IEEE Trans. Commun.*, vol. 61, no. 10, pp. 4391–4403, Oct. 2013.
- [10] A. F. Molisch, *Wireless Communications*. Wiley, 2012, vol. 34.
- [11] A. Alkhateeb, O. El Ayach, G. Leus, and R. W. Heath, "Channel estimation and hybrid precoding for millimeter wave cellular systems," *IEEE J. Sel. Topics Signal Process.*, vol. 8, no. 5, pp. 831–846, Oct. 2014.
- [12] D. Zhu, J. Choi, and R. W. Heath, "Auxiliary beam pair enabled aod and aoa estimation in closed-loop large-scale millimeter-wave MIMO systems," *IEEE Trans. Wireless Commun.*, vol. 16, no. 7, pp. 4770–4785, Jul. 2017.
- [13] T. E. Bogale, L. B. Le, and X. Wang, "Hybrid analog-digital channel estimation and beamforming: Training-throughput tradeoff," *IEEE Trans. Commun.*, vol. 63, no. 12, pp. 5235–5249, Dec. 2015.
- [14] A. Alkhateeb, G. Leus, and R. W. Heath, "Compressed sensing based multi-user millimeter wave systems: How many measurements are needed?," in *Proc. IEEE Int. Conf. Acoust., Speech Signal Process.*, 2015, pp. 2909–2913.
- [15] Z. Gao, L. Dai, Z. Wang, and S. Chen, "Spatially common sparsity based adaptive channel estimation and feedback for FDD massive MIMO," *IEEE Trans. Signal Process.*, vol. 63, no. 23, pp. 6169–6183, Dec. 2015.
- [16] J. Lee, G. Gil, and Y. H. Lee, "Channel estimation via orthogonal matching pursuit for hybrid MIMO systems in millimeter wave communications," *IEEE Trans. Commun.*, vol. 64, no. 6, pp. 2370–2386, Jun. 2016.
- [17] T. T. Cai and L. Wang, "Orthogonal matching pursuit for sparse signal recovery with noise," *IEEE Trans. Inf. Theory*, vol. 57, no. 7, pp. 4680–4688, 2011.
- [18] Z. Zhou, J. Fang, L. Yang, H. Li, Z. Chen, and R. S. Blum, "Low-rank tensor decomposition-aided channel estimation for millimeter wave MIMO-OFDM systems," *IEEE J. Sel. Areas Commun.*, vol. 35, no. 7, pp. 1524–1538, Jul. 2017.
- [19] Z. Zhou, J. Fang, L. Yang, H. Li, Z. Chen, and S. Li, "Channel estimation for millimeter-wave multiuser MIMO systems via parafac decomposition," *IEEE Trans. Wireless Commun.*, vol. 15, no. 11, pp. 7501–7516, Nov. 2016.
- [20] X. Li, J. Fang, H. Li, and P. Wang, "Millimeter wave channel estimation via exploiting joint sparse and low-rank structures," *IEEE Trans. Wireless Commun.*, vol. 17, no. 2, pp. 1123–1133, Feb. 2018.
- [21] E. Vlachos, G. C. Alexandropoulos, and J. Thompson, "Massive MIMO channel estimation for millimeter wave systems via matrix completion," *IEEE Signal Process. Lett.*, vol. 25, no. 11, pp. 1675–1679, Nov. 2018.
- [22] T. Oh, Y. Matsushita, Y. Tai, and I. S. Kweon, "Fast randomized singular value thresholding for low-rank optimization," *IEEE Trans. Pattern Anal. Mach. Intell.*, vol. 40, no. 2, pp. 376–391, Feb. 2018.
- [23] R. W. Heath, N. Gonzalez-Prelcic, S. Rangan, W. Roh, and A. M. Sayeed, "An overview of signal processing techniques for millimeter wave MIMO systems," *IEEE J. Sel. Topics Signal Process.*, vol. 10, no. 3, pp. 436–453, Apr. 2016.
- [24] R. Hu, J. Tong, J. Xi, Q. Guo, and Y. Yu, "Matrix completion-based channel estimation for mmwave communication systems with array-inherent impairments," *IEEE Access*, vol. 6, pp. 62 915–62 931, 2018.
- [25] M. R. Akdeniz *et al.*, "Millimeter wave channel modeling and cellular capacity evaluation," *IEEE J. Sel. Areas Commun.*, vol. 32, no. 6, pp. 1164–1179, Jun. 2014.
- [26] I. A. Hemadeh, K. Satyanarayana, M. El-Hajjar, and L. Hanzo, "Millimeter-wave communications: Physical channel models, design considerations, antenna constructions, and link-budget," *IEEE Commun. Surv. Tutorials*, vol. 20, no. 2, pp. 870–913.
- [27] E. Vlachos, G. C. Alexandropoulos, and J. Thompson, "Wideband MIMO channel estimation for hybrid beamforming millimeter wave systems via random spatial sampling," *IEEE J. Sel. Topics Signal Process.*, vol. 13, no. 5, pp. 1136–1150, 2019.
- [28] E. J. Candes and M. B. Wakin, "An introduction to compressive sampling," *IEEE Signal Process. Mag.*, vol. 25, no. 2, pp. 21–30, Mar. 2008.
- [29] N. Jain, V. A. Bohara, and A. Gupta, "iDEG: Integrated data and energy gathering framework for practical wireless sensor networks using compressive sensing," *IEEE Sensors J.*, vol. 19, no. 3, pp. 1040–1051, Feb. 2019.
- [30] N. Jain, A. Gupta, and V. A. Bohara, "PCI-MDR: Missing data recovery in wireless sensor networks using partial canonical identity matrix," *IEEE Wireless Commun. Lett.*, vol. 8, no. 3, pp. 673–676, Jun. 2019.
- [31] I. W. Selesnick, "Sparse signal restoration," *Connexions*, pp. 1–13, 2009.
- [32] A. Beck and M. Teboulle, "A fast iterative shrinkage-thresholding algorithm for linear inverse problems," *SIAM J. Imag. Sci.*, vol. 2, no. 1, pp. 183–202, 2009.
- [33] S. Boyd *et al.*, "Distributed optimization and statistical learning via the alternating direction method of multipliers," *Found. Trends Mach. Learn.*, vol. 3, no. 1, pp. 1–122, 2011.
- [34] Z. Wen, W. Yin, and Y. Zhang, "Solving a low-rank factorization model for matrix completion by a nonlinear successive over-relaxation algorithm," *Math. Program. Comput.*, vol. 4, no. 4, pp. 333–361, Dec. 2012. [Online]. Available: <https://doi.org/10.1007/s12532-012-0044-1>
- [35] J. G. Andrews, T. Bai, M. N. Kulkarni, A. Alkhateeb, A. K. Gupta, and R. W. Heath, "Modeling and analyzing millimeter wave cellular systems," *IEEE Trans. Commun.*, vol. 65, no. 1, pp. 403–430, Jan. 2017.
- [36] M. Polese and M. Zorzi, "Impact of channel models on the end-to-end performance of mmwave cellular networks," in *Proc. IEEE 19th Int. Workshop Signal Process. Adv. Wireless Commun.*, 2018, pp. 1–5.
- [37] T. S. Rappaport *et al.*, "Millimeter wave mobile communications for 5G cellular: It will work!," *IEEE Access*, vol. 1, pp. 335–349, 2013.
- [38] T. Yoo and A. Goldsmith, "Capacity of fading MIMO channels with channel estimation error," in *Proc. IEEE Int. Conf. Commun.*, vol. 2, 2004, pp. 808–813.
- [39] D. M. Tarique and M. T. Hasan, "Article: Impact of Nakagami-m fading model on multi-hop mobile ad hoc network," *Int. J. Comput. Appl.*, vol. 26, no. 2, pp. 5–12, Jul. 2011, full text available.
- [40] N. Jain and V. A. Bohara, "Energy harvesting and spectrum sharing protocol for wireless sensor networks," *IEEE Wireless Commun. Lett.*, vol. 4, no. 6, pp. 697–700, Dec. 2015.